NANO MICRO small

Supporting Information

for *Small*, DOI: 10.1002/smll.202003141

Modal Frustration and Periodicity Breaking in Artificial Spin Ice

Robert Puttock, Alessandra Manzin, Volker Neu, Felipe Garcia-Sanchez, Alexander Fernandez Scarioni, Hans W. Schumacher, and Olga Kazakova*

Supplementary Information: Modal frustration and periodicity breaking in artificial spin ice

Authors: R. Puttock[1,2], A. Manzin[3], V. Neu[4], F. Garcia-Sanchez[3,5], A. Fernandez Scarioni[6], H. W. Schumacher[6], and O. Kazakova[1].

Affiliations: [1]*National Physical Laboratory, Teddington TW11 0LW, United Kingdom.* [2]*Department of Physics, Royal Holloway University of London, Egham Hill, Egham TW20 0EX, United Kingdom.* [3]*Istituto Nazionale di Ricerca Metrologica, Torino 10135, Italy.* [4]*Leibniz Institute for Solid State and Materials Research, Dresden 01069, Germany.* [5]Departamento de Física Aplicada, University of Salamanca, Pza de la Merced s/n, 37008 Salamanca, Spain. [6]*Physikalisch-Technische Bundesanstalt, Braunschweig 38116, Germany.*

S1: Determination of the easy and hard axes of the ASI lattice via micromagnetic modelling

To investigate the shape anisotropy properties of the studied ASI lattice, we perform a detailed micromagnetic modelling analysis, calculating the remanence magnetization value as a function of the applied field orientation. We start from a saturation state along a direction that forms an angle β with respect to the *x*-axis and leave the ASI system to evolve up to remanence, by gradually reducing the field along the same direction. We deduce that the ASI lattice is characterized by a nearly two-fold anisotropy with the easy axes at 90° and at the equivalent direction (β = 270°). The hard axes coincide with the angular orientations of 0° and 180°. An intermediate behavior is found for β = 45°, 135°, 225° and 275°, due to the presence of NIs orientated along these directions.

The high remanence value, close to saturation, is obtained with β = 90° (easy axis). In this case, the ASI lattice is characterized by a periodic magnetic state, with the magnetization spatial distribution following the NI longitudinal axes. This magnetic state is maintained up to β = 45°, where shape anisotropy effects occurring in the NIs close to the boundaries give rise to a partial reversal of the magnetization in the peripheral NIs. For β between 45° and 0°, we find again a periodical spatial distribution of the magnetization, with the NIs along the 135° direction characterized by a partial rotation of the magnetization, which results orientated at -45°.

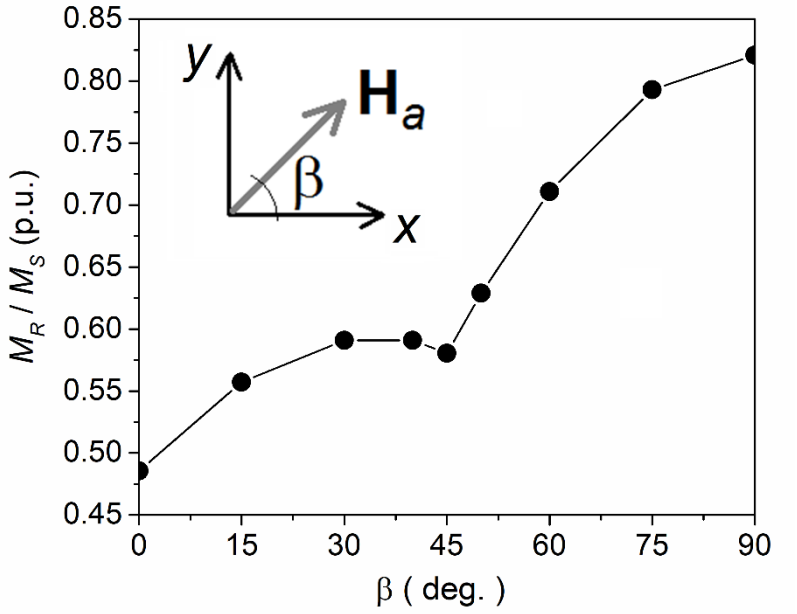

S1. **Determination of easy and hard axes.** Calculated remanence magnetization value (normalized to saturation), as a function of the angle β of the applied field with respect to the *x*-axis (see inset)

S2: MFM images of QH-lattice for Figure 2 of the main manuscript

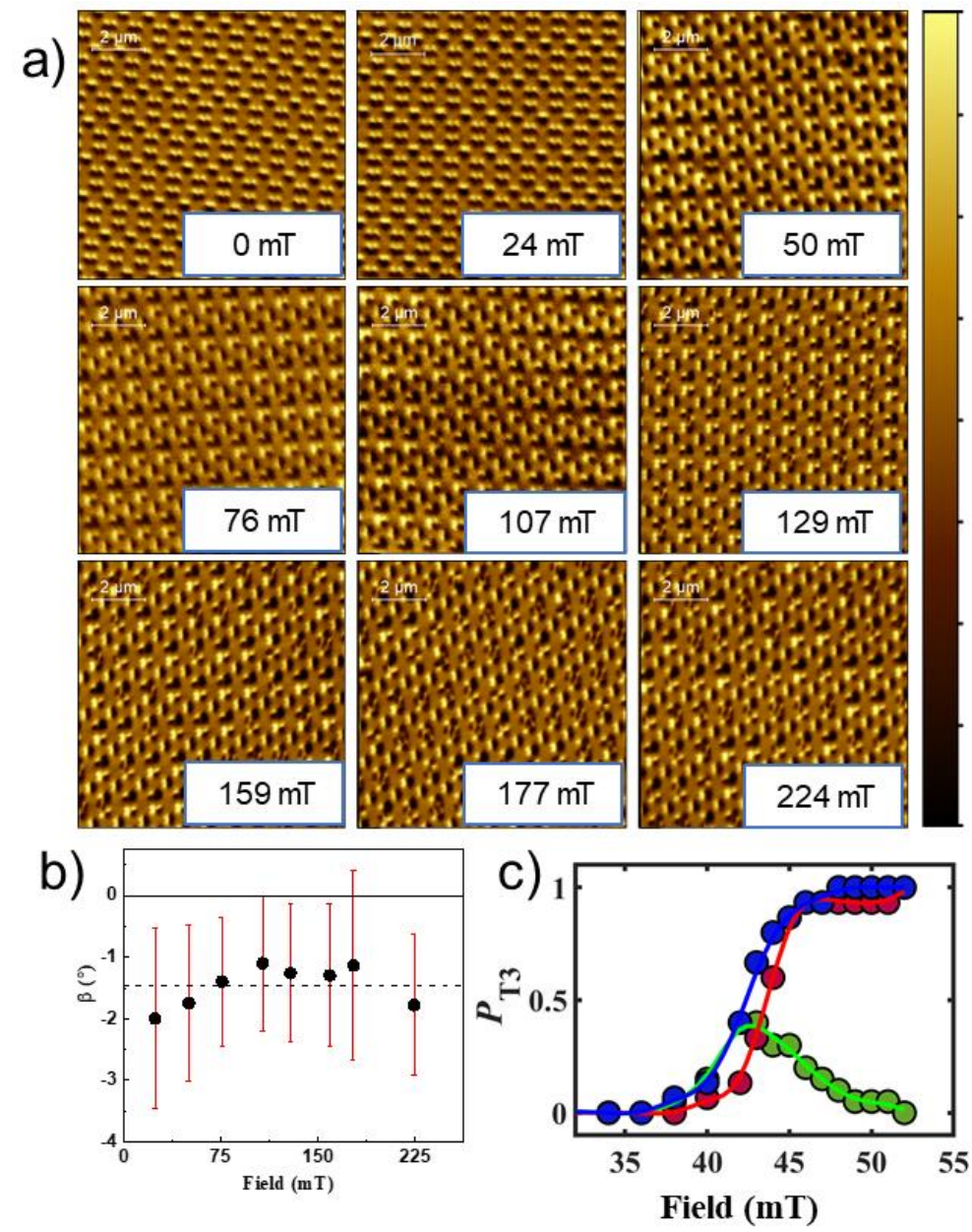

***S2*. (a) Experimental MFM images at remanence after field application.** 10×10 μm MFM images taken at remanence at the center of the QH-lattice post application of specified field along the hard-axis of the lattice; switching from unimodal, to bimodal and finally to a multimodal state. **(b)** The field angle (β) and uncertainty (2σ) for each field magnitude applied to the sample. (c) Population frequency of T_3 energy states across X (green), Y (red) and rY (blue) vertices within the field-range 35-50 mT, demonstrating a two-step transition between uni- and bimodal states.

S3: Analysis of the transition from uni- to multimodal state via micromagnetic modelling

The magnetisation maps and diagrams depicted in this figure directly correlate to figure 3a-c in the main manuscript.

(a) QH-ASI with 1× separation

Here we focus on the determination, via micromagnetic modelling, of the field conditions leading to the transition from uni- to bimodal state. To this aim, we mimic the experimental conditions, by first demagnetizing the ASI nanostructure along the *y*-axis (Fig. S3ai). Py saturation magnetization M_s = 860 kA/m, and an exchange constant J = 13 pJ/m were used. In addition, contributions from magnetocrystalline anisotropy and thermal noise were considered to be negligible for Py and excluded from the calculation. The remanence magnetization configuration obtained after the demagnetization process is characterized by a periodic distribution of unimodal T_2 states, where the magnetization in the longitudinal NIs is reversed [Fig. S3aii(i)]. Starting from this ground state we apply an *x*-orientated magnetic field, following the sequence adopted in the measurements, i.e. at each field increment the field is increased up to the set-value and then reduced to zero. The remanence bimodal state appears after the application of a field of 75 mT, as illustrated by Fig. S3aii(ii), while a distribution of matching and non-matching chiral Landau states forms after the application of a field of 275 mT (S3aii(iii)).

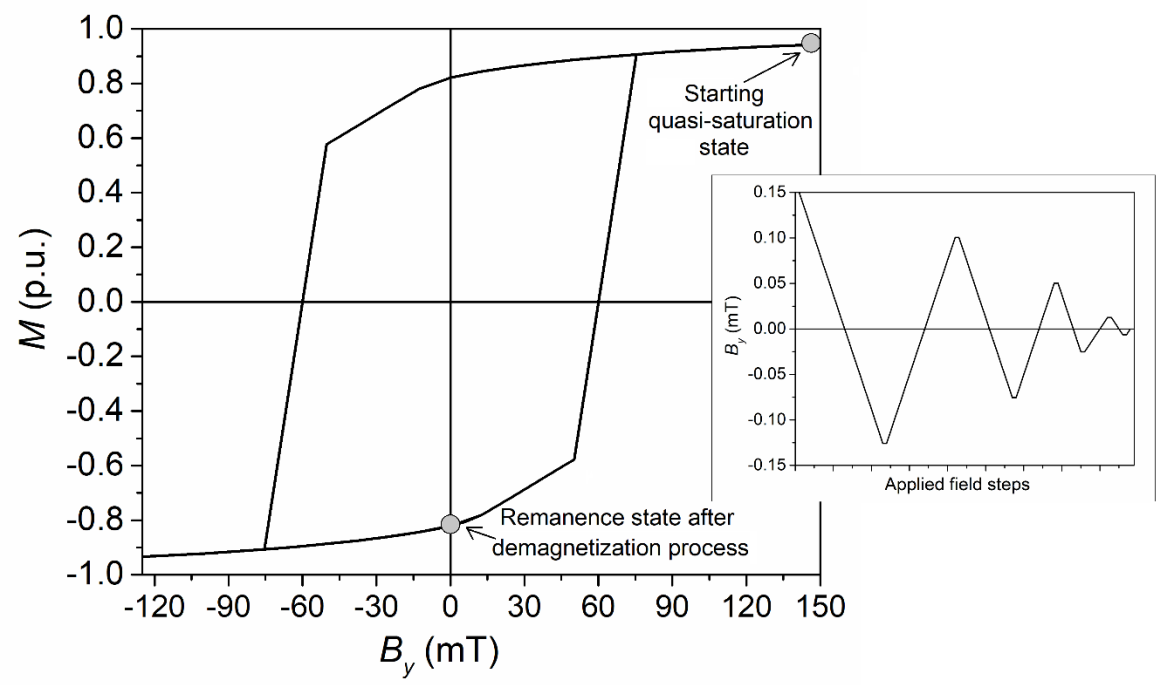

S3ai. Simulated M(B) curve. Magnetization versus applied field during the demagnetization process along the easy direction (*y*-axis). The schematic of the demagnetization procedure is depicted in the inset.

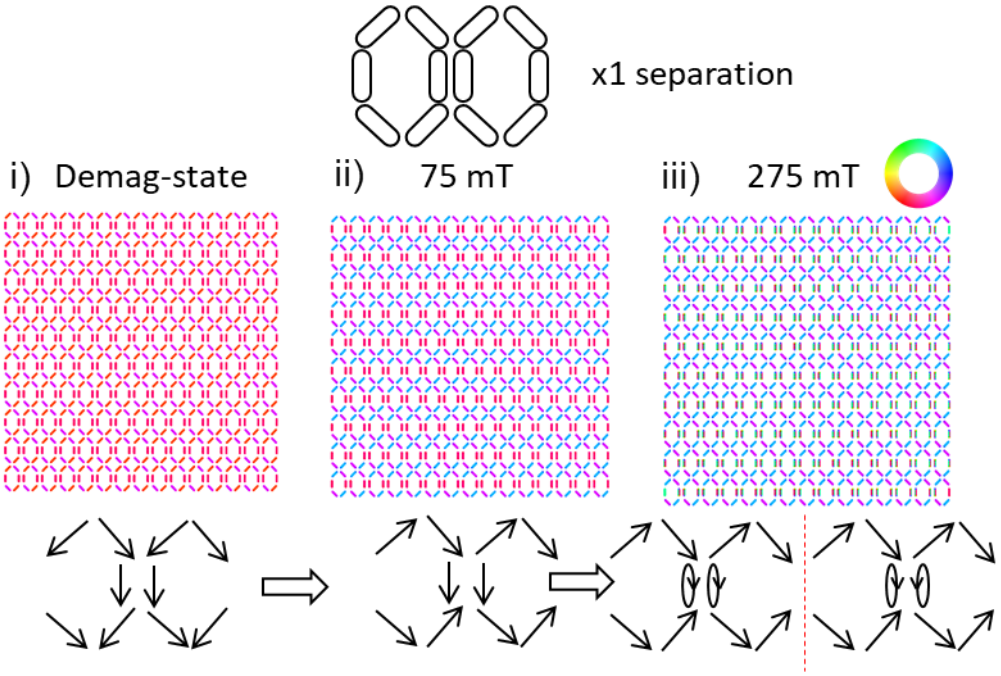

S3aii. Remanence magnetization configurations calculated for the QH-ASI lattice with nominal separation following the field sequence described in the main manuscript (Fig. 3). (i) initial state after demagnetization process along *y*-axis and the application of an *x*-orientated field magntidue: (ii) 75 mT and (iii) 275 mT, which corresponds to the uni-, bi- and multimodal states, respectively. The color wheel represents the angle that the magnetization vector forms with the *x*-axis.

(b) QH-ASI with 0.5× separation distance

Here, we measure the modelled evolution of the energy landscape under the field protocol outlined in the main manuscript when the interisland separation in the QH lattice is reduced by half. Directly comparing with the dataset outlined in Fig. S3aii, the profile of the energy evolution broadly follows the same trajectory, except for an additional step upon the first formation of the Landau states. Starting from the UM state (S3b(i)), the field required to form the BM state (S3b(ii)) is ~100 mT, which is greater than required for the original dataset in S3a(ii). The closer inter-island separation increases the energy barrier between the two modal configurations, therefore more field is required to form the higher energy configuration. Contrarily, The LSs form more readily in the lattice with reduced separation as a two-step formation is shown in (S3b(iii)) and (S3b(iv)). State (iii) formed at (~200 mT) shows a magnetic configuration that was not previously seen in the dataset displayed in Fig. S3aii, where a mix of Ising and non-Ising states are stable across the QH-lattice. State S3b(iv) matches the same configuration described in Fig. S3aii(iii), where all NIs (except those in the corners due to the symmetry-breaking) are LSs of mixed chirality. The configuration in (S3b(iii)) perhaps resembles the experimentally observed MM configuration more closely than the original model. As the resolution capacity of e-beam lithography is on the order of 10's nm (due to scattering, or beam broadening etc.) it is likely that the NIs are closer together than the original 2D-CAD designs, which were used for the micromagnetic simulations.

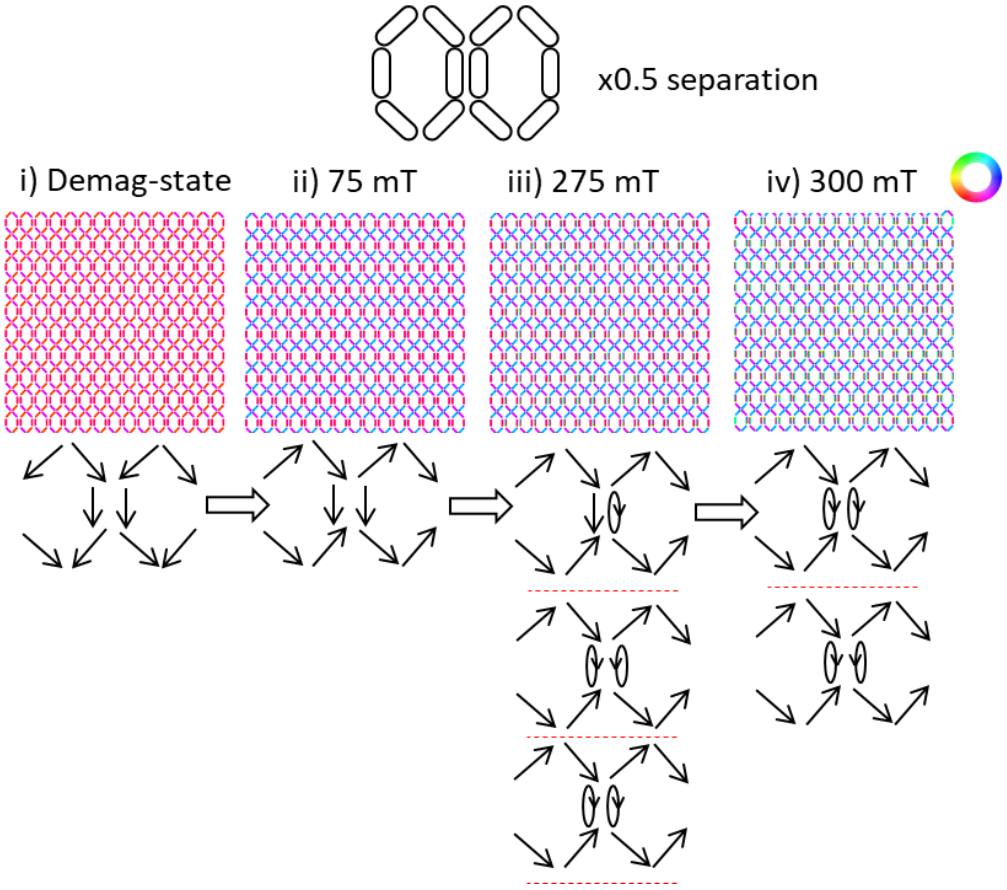

S3b. Remanence magnetization configurations for the QH-ASI lattice, at half inter-island separation, calculated following the field sequence described in the main manuscript. (i) initial state after demagnetization process along *y*-axis and the application of an *x*-orientated field magntidue: (ii) 100 mT, (iii) 200 mT (iv) 300 mT, which corresponds to the uni-, bi- and multimodal states, respectively. The color wheel represents the angle that the magnetization vector forms with the *x*-axis.

(c) QH-ASI with 1× separation distance and no parallel islands

Here, we focus on understanding the magnetic evolution of a hexagonal lattice, without coupled-parallel nanomagnets, via micromagnetic modelling. This means that the Y/rY junctions are formed of three NIs. We mimic the experimental conditions of the main manuscript by first demagnetizing the ASI nanostructure along the *y*-axis (Fig. S3c(i)). The starting magnetization configuration is characterized by a periodic distribution of high-energy states, where the magnetic configuration at each Y/rY vertex is *three-in* or *three-out*; and *two-in two-out* in the X-Shaped vertices. We subsequently apply an *x*-orientated magnetic field, following the sequence adopted in the measurements, i.e. at each step the field is gradually increased up to the quoted level and then reduced to zero. The first change in the magnetic landscape is generated upon the application of a field of 75 mT (S3c(ii)) where the X-Shaped vertices reorient their net-magnetic moment to align along the incident field direction. This relaxes the Y-/rY vertices into a *two-in one-out* energy state, or vice versa, respectively. Landau states, all with the same chirality, are formed after the application of a field of 275 mT (S3c(iii))), the same field magnitude as is shown from the micromagnetic simulations of the original QH-lattice in S3aii. At the next field increment (300 mT), we see a new transition from uniform Landau states back to fully Ising states (Fig. S3c(iv)), aside from some Landau states which remain at the edges of the modeled lattice. Here the nanoislands perpendicular to the field are magnetically aligned in the opposite direction to the initial remanent state of S3c(i).

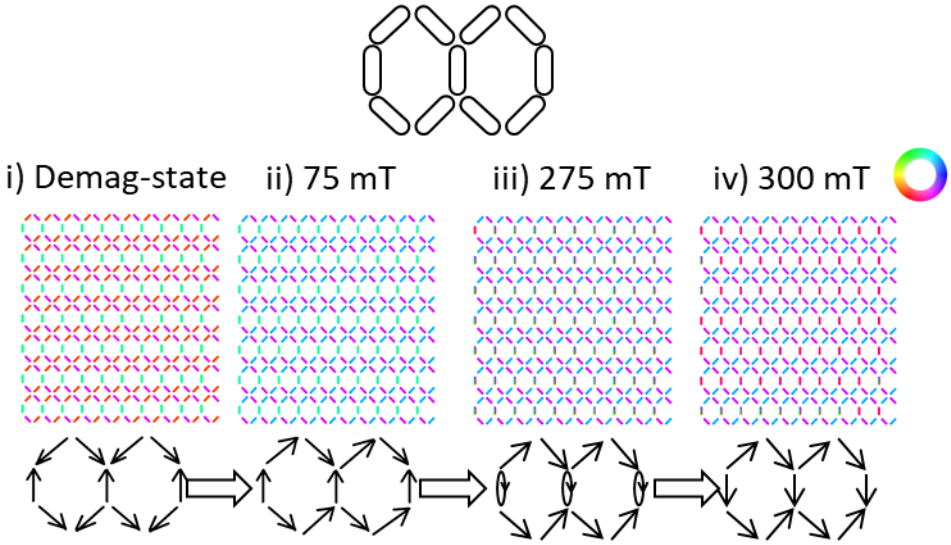

S3c. Remanence magnetization configurations calculated along the field sequence shown in the main manuscript on a lattice without coupled parallel islands. (i) Initial state after the demagnetization process along *y*-axis, and the application of an *x*-orientated field of (ii) 75 mT, (iii) 275 mT and (iv) 301 mT. The color wheel represents the angle that the magnetization vector forms with the *x*-axis. Schematics of the NI magnetization are included for reference.

S4: Experimental comparison with other ASI lattices

Additional population frequency measurements on traditional ASI structures of the same NI dimensions. The additional designs chosen were the traditional square lattice and the 3D-Square lattice, replicated from Wang *et al*[1]. These two datasets (S4b) were taken under the exact same experimental conditions as was utilized in the manuscript. A complementary dataset (S4b) was taken for the QH- and 3D Square lattices under the same experimental protocol, but the field angle was not monitored throughout the field protocol.

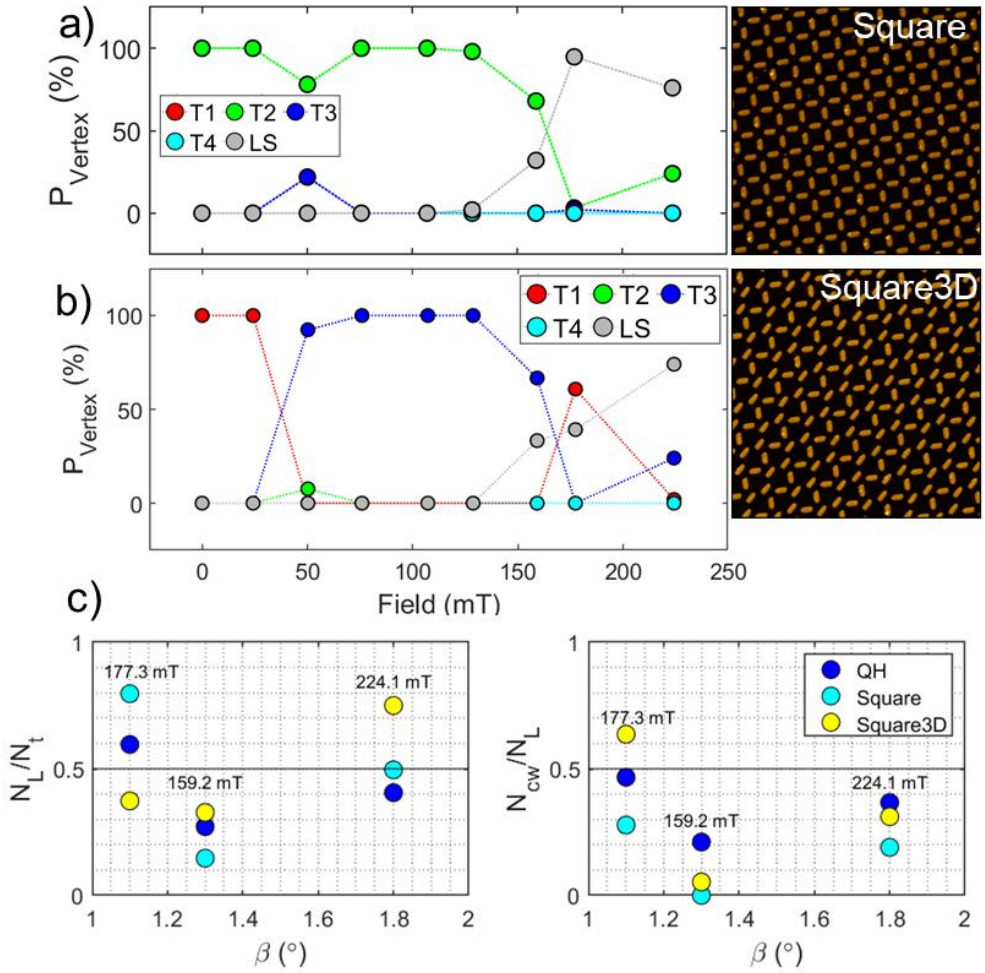

S4a. Population frequency of each magnetic configuration per vertex, and topography image of Square (a) and 3D-Square (b) lattices as a function of field applied along the *x*-direction of the lattice after an initial demagnetisation protocol along the *y*-axis. Angle of the field vector is shown in Figure S2(b). Initial Ising-Ising switching occurs around the same field magnitude (approx. 50 mT) as for the QH-Lattice. Landau states (LSs) begin to form in the lattices in the *y*-oriented NIs at $B > 150$ mT. Normalized number of LSs (c) and normalised number of CW LSs (d) in QH, Square, and 3D-Square ASI as a function of field angle and magnitude. The field magnitude at $B = 159$ mT appears to be the more dominant variable over the angle, causing a reduction in both the number of LSs and CW LSs in the image. The number of LSs in 3D-Square ASI declines with field angle due to a larger number of full Ising-switching events at $B = 177$ mT, which in turn generates a greater amount of T1 energy states shown in (b). Under all field magnitude and angle combinations, QH-lattice demonstrates the most even split in CW-to-CCW Landau states from the coupled NI dispersion.

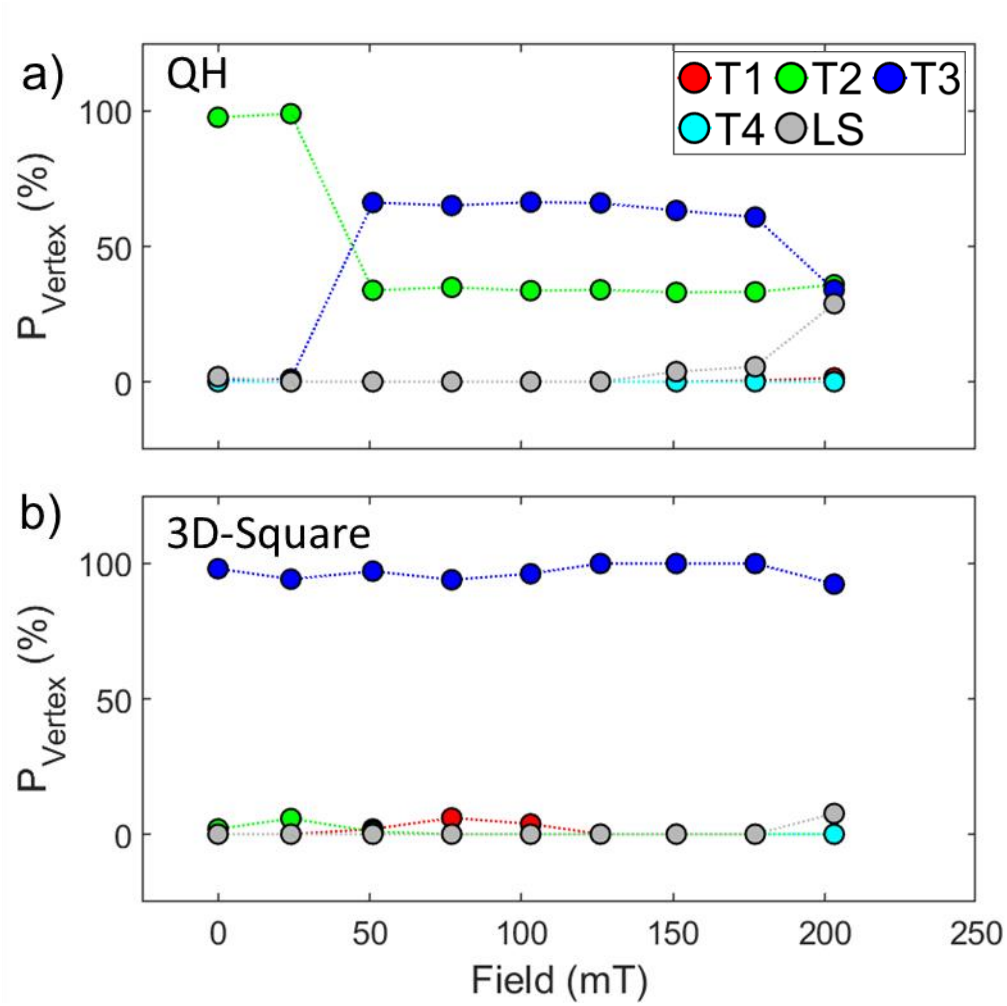

S4b. Vertex population of QH (a) and 3D-Square (b) lattices as a function of field applied along the *x*-direction of the lattice after an initial demagnetisation protocol along the *y*-axis. Here, the field angle off of the hard-axis direction was not measured or controlled. The data demonstrates the same uni- and bimodal behaviours, and the lack thereof, in the QH and 3D-Square lattice respectively. Landau states begin to form in the QH-lattice around similar field magnitudes as the dataset in the main manuscript, though in smaller quantity.

S4: Micromagnetic modelling of an individual island

To calculate the energy cost of the formation of the LS in an isolated nanoisland, further micromagnetic modelling was performed. This was conducted in the Object-oriented micromagnetic framework (OOMMF) open source software maintained by NIST.[2] The same material parameters of M_s = 860 kA/m, and an exchange constant J = 13 pJ/m were used, in the absence of thermal noise. The island was a stadium geometry of width w=100 nm, height h=380 nm and a thickness of t=24 nm. As OOMMF operates using FFT methods for its calculations changing the thickness to be a multiple of 2 helped to speed up the simulations. In addition, the damping parameter α was set at 0.5 to speed-up the convergence time, which is nominally higher than the α used in the previous modelling. The nanoelement was discretized into cubes of size 2×2×2 nm for the time-evolved simulations. The results are summarized in the magnetization maps in figure S5.

S5(a) and (b) show the initial and relaxed magnetisation configurations for two instances where the magnetization is highly deviated from a typical single domain nanoelement. The initial configuration is S5(a) is a full saturation along the in-plane hard-axis of the nanoelement. Upon relaxation, the

model converged into a single-domain nanoelement. The same result (albeit inverted) when the initial configuration was set randomized was also achieved.

Figure S5c shows the final converged configuration after forcing the magnetization of the nanoelement to be single-domain (left) and multi-domain (right). Here the relative total energy densities are displayed alongside the converged magnetization maps. The energy difference is almost two-fold between the multi and single-domain state, indicating that its formation is not energetically favorable. From these values, we can calculate the energy cost of being in this magnetic configuration as as 38879 – 21825 J/m^3 = 17054 J/m^3.

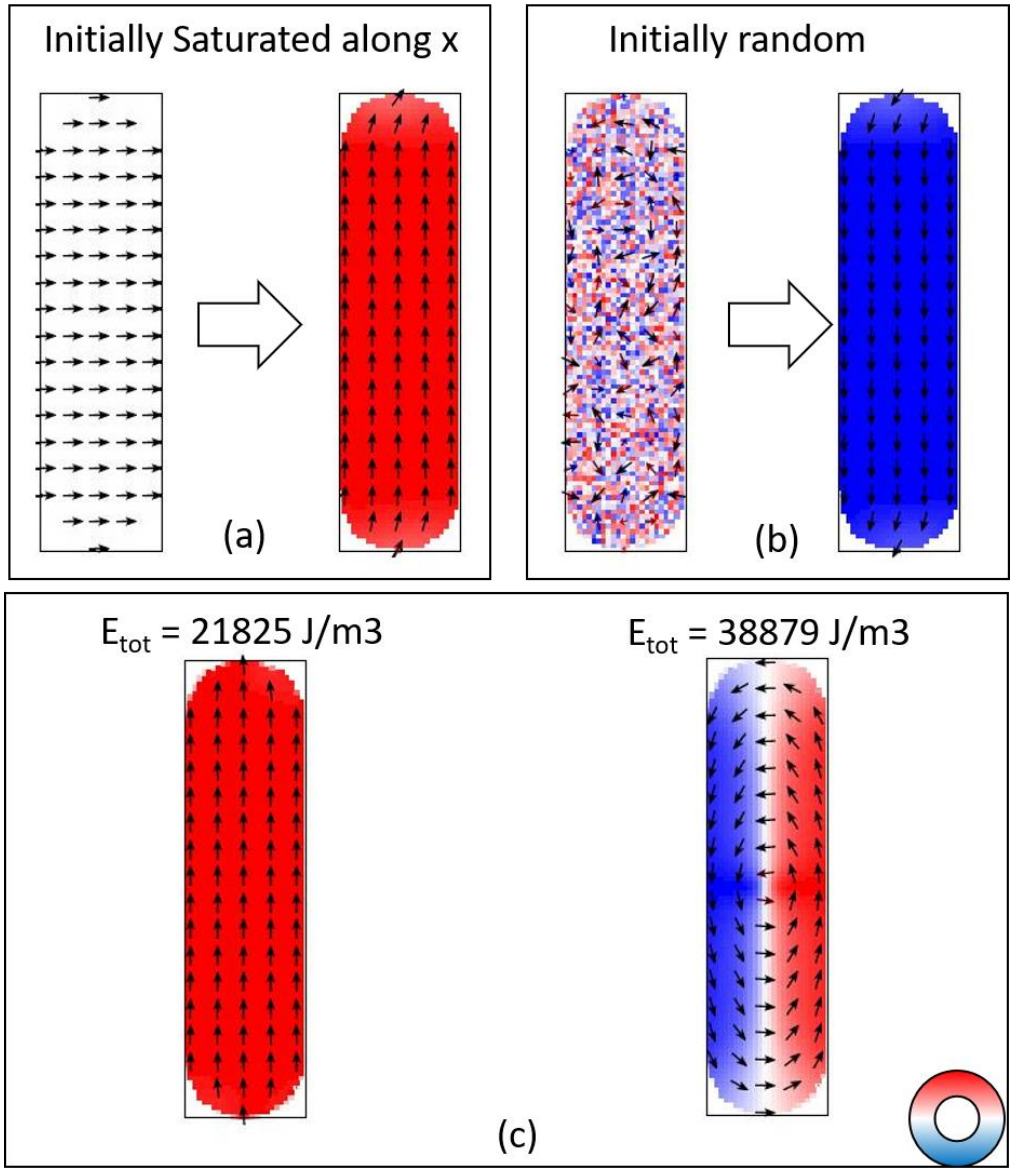

S5. (a) Initial and final (converged) magnetization maps for a stadium-geometry nanoelement when initially saturated along the in-plane hard axis. (b) Initial and final (converged) magnetization maps for a stadium-geometry nanoelement when initially the magnetization is randomized. (c) Converged magnetization maps when the initial magnetization of the nanoelement was single- and multi-domain (left and right, respectively), alongside their respective total energies. The colorwheel represents the m_y component of the magnetisation.

1. Wang, Y.-L. *et al.* Rewritable artificial magnetic charge ice. *Science (80-.).* **352**, 962–966 (2016).

2. Porter, D. G. & Donahue, M. J. *OOMMF User's Guide, Version 1.0*. http://math.nist.gov/oommf (1999).